BNL-82220-2009-JA

RETRIEVAL OF CLOUD LIQUID WATER DISTRIBUTIONS FROM A SINGLE SCANNING MICROWAVE RADIOMETER ABOARD A MOVING PLATFORM. PART II: OBSERVATION SYSTEM SIMULATION EXPERIMENTS

Huang, D.[1*], Gasiewski, A.[2], and Wiscombe, W.[1,3]

[1] Brookhaven National Laboratory, Upton, NY 11973
[2] University of Colorado, Boulder, CO 80309
[3] NASA Goddard Space Flight Center (code 913), Greenbelt, MD 20771
* Corresponding author: Dong Huang, Brookhaven National Laboratory, Atmospheric Sciences Division, Bldg. 815E, 75 Rutherford Drive, Upton, NY 11973; Telephone: (631) 344-5818; Email: dhuang@bnl.gov

Submitted for publication in
Atmos. Chem. Phys.

April 2009

Environmental Sciences Department/Atmospheric Sciences Division

Brookhaven National Laboratory
P.O. Box 5000
Upton, NY 11973-5000
www.bnl.gov

DISCLAIMER

Abstract

Part I of this research reveals that many conditions of the 2003 cloud tomography experiment at the Wakasa Bay were not ideal for the tomographic retrieval purpose. For example, the aircraft flew too fast and its altitude was too high. Part II (this paper) then focuses on the examination of several possible improvements on the mobile cloud tomography method by means of observation system simulation experiment. We find that the incorporation of the L_1 norm total variation regularization in the tomographic retrieval algorithm better reproduces small scale discontinuous structure than the widely used L_2 norm Tikhonov regularization and successfully resolves sharp cloud edges. The simulation experiments reveal that a typical ground-based mobile cloud tomography setup substantially outperforms an airborne one because of its slower moving speed and greater contrast in microwave brightness between clouds and the cosmic background. The simulations show that, as expected, the retrieval error increases monotonically with radiometer noise level and the uncertainty in background brightness temperature. It is also revealed that a slower platform or a faster scanning radiometer results in more scan cycles and better overlapping between the swaths of successive scan cycles, both of which are highly favorable for cloud tomography retrieval. The last factor examined is aircraft height. It is shown that the best retrieval is obtained when the aircraft data are collected at the altitudes between 500 meters to 1000 meters above the cloud top. To summarize, this research demonstrates the feasibility of tomographically retrieving cloud structure using current scanning microwave radiometer technology and provides several general guidelines by which to improve future field-based studies of cloud tomography.

1. Introduction

Clouds in the lower troposphere exert enormous influences on the Earth's radiation budget and also play a crucial role in the planet's hydrological cycle. The spatial distribution of cloud water is one of the most poorly represented component and is considered as one of the largest uncertainties in the predictions of climate change by numerical models (Weare, 1996; Stephens, 2005). Part of the reason is that the scarcity of long-term consistent cloud observations makes it hard to derive accurate cloud statistics. Existing techniques can hardly provide adequate measurements of clouds at the temporal and spatial resolution required by the study of radiation and cloud physical processes. In order to evaluate thus to improve cloud representations in numerical models, we need observation techniques that are capable of providing accurate cloud data at suitable temporal and spatial resolution. Aircraft-based in-situ measurements can only sample a small volume of a cloud, while the widely used vertical-pointing radiometers, such as those used in the Department of Energy ACRF sites, are capable of measuring only the vertical integral of the Liquid Water Content (LWC) (Liljegren et al., 2001; Westwater et al., 2004). On the other hand, active remote sensing techniques like cloud radar (Frisch et al., 1995; Hogan et al., 2005) with rapid scanning capability provide a less direct measurement of cloud water content (since radar reflectivity depends strongly on the particle size distribution) and also would likely be much more costly than passive methods.

Microwave tomographic methods provide a new promise for the cloud observation problem. It was first proposed in 1980s that cloud tomography measurements can be made either by multiple distinctly-located ground microwave radiometers or by a single

radiometer boarded on a mobile platform. The reconstruction of cloud water distribution from the tomographic measurements can be converted into a matrix inversion problem (Warner et al., 1985; Drake and Warner, 1988; and Warner and Drake, 1988). The fixed ground-based configuration has the apparent advantage that it can operate continuously without human intervention and thus it is suitable for long-term deployment. It was revealed recently that the quality of cloud reconstruction is depended on the number of microwave radiometer as well as their physical arrangement (Huang et al., 2008a). At least four ground radiometers are needed for the fixed configuration to obtain a cloud reconstruction that is accurate to within 10% of the cloud's maximum water content. The requirement for a large number of microwave radiometers makes the fixed tomography configuration expensive to deploy. Furthermore, the lack of cloud chasing capability limits the usage of the fixed configuration in applications that require efficient data collection like a field campaign.

Alternatively, a mobile tomography configuration with a moving platform needs only one scanning radiometer to collect tomographic data of the similar quality. Geometrically, a tomographic reconstruction would require the object (it is clouds for cloud tomography) to be scanned from multiple locations and directions. In other words, two scanning mechanisms are needed: spatial scan and angular scan. The spatial scanning of clouds is achieved in a mobile configuration by the horizontal movement of the platform instead of using multiple distinctly-located radiometers. A first investigation of the mobile configuration was performed by Drake and Warner (1988), in which the radiometer switches automatically between two fixed antennas as the platform moves along a horizontal line passing just under a cloud. They showed that the configuration with two

fixed antennas performed similarly as a ground-based tomography configuration using two scanning radiometers. A follow-up field test was carried out in Louisiana and the LWC deduced from the radiometric measurements showed statistically good agreement with that measured directly by an airborne Particle Measurement System but a point-by-point comparison was not made because of scale mismatch of the two measurement techniques (Warner and Drake, 1988).

It was shown that for cloud tomography the number of directions each cloud pixel being viewed is one of the most important factors (Huang et al., 2008). The use of dual-antenna in Warner's setup (not a scanning radiometer in a strict sense) allows for only two view directions, which is far from optimal and would result in very insufficient information in the radiometric data to retrieve the cloud structure (Huang et al., 2008a). The angular sampling of clouds can be improved by replacing the dual-antenna radiometer with a real scanning radiometer that can scan continuously at different elevation and azimuth angles while the platform passing the interested cloud.

A very limited cloud tomography experiment was conducted during the 2003 AMSR-E validation campaign at Wakasa Bay of the sea of Japan (Lobl et al., 2007), where the Polarimetric Scanning Radiometer (PSR) was mounted under the NASA P-3 research aircraft and scanned through a system of low-altitude clouds from above (Piepmeier and Gasiewski, 1996). Part I of this research revealed that the tomographically retrieved cloud water fields roughly capture the spatial features of clouds compared with a radar image, but a lot of high-frequency cloud structure is missed in the retrievals. It was found that many conditions of the Wakasa Bay experiment were not optimal for cloud tomography retrieval, such as strong surface wind and high aircraft speed. A more thorough

examination of the mobile tomography method is thus needed in order to determine the optimal conditions and data collection strategies. These are the focus of Part II (this paper) of this research.

Two possible mobile configurations are considered in this paper: an airborne configuration and a ground-based configuration (Figure 1). The first configuration uses an aircraft as the mobile platform; this is the configuration used in the cloud tomography test during the 2003 AMSR-E validation campaign at the Wakasa Bay. The microwave radiometer is mounted under the aircraft, which is a typical design of research aircrafts. With this design, the aircraft has to fly from above the interested clouds in order to measure their thermal emission. Figure 1a shows the swaths of three successive scan cycles, each labeled in different color. The aircraft translates a certain distance along the flight track during each scan cycle, and the location of the aircraft for each cycle is also shown in the same figure with matching color. The other configuration shown in Figure 1 is ground-based and it makes use of a pickup truck. Four scan cycles are shown for the ground-based configuration, suggesting that the slower ground-based platform usually allows for more scan cycles than its airborne counterpart within the same distance. In both configurations, the radiometer scans within the vertical plane of the platform path. More details on the difference between the ground-based and airborne configurations and their relevance to cloud tomography retrieval are described in Section 4.

The paper is organized as follows. In Section 2 we present the details of the observation system simulation experiment of cloud tomography. Section 3 examines the skill of two different retrieval algorithms: one based on the standard Tikhonov regularization and the other based on the total variation regularization. Section 4 presents

a group of sensitivity tests and thus provides useful guidelines for possible improvement on the mobile cloud tomography method. Section 5 summarizes the findings of this study.

2. Description of methodology

Observation system simulation experiment is a useful tool to study a forecast or retrieval system. The observation system simulation for cloud tomography is mainly composed of two components: a forward model to generate some virtual cloud microwave tomography measurements and an inverse algorithm to retrieve cloud water fields from the simulated radiometric measurements. The forward model is an algorithm for sampling modeled clouds in a manner consistent with the way microwave radiometers observe. Specifically, the forward model first generates some test clouds using a large eddy simulation model, and then simulates microwave measurements with some prescribed radiometer specifications using a radiative transfer equation in a way consistent with radiometers observe.

In order to examine the validity of the mobile cloud tomography method under different environmental conditions, we select two very different cloud cases as the basis of the observation system simulation experiments (Figure 2). The first case is a mid-latitude stratocumulus cloud simulated by the DHARMA large eddy simulation model driven by data from Atlantic Stratus Experiment (ASTEX) (Ackerman et al., 1995). The stratocumulus clouds in the ASTEX region generally have cloud tops between the 800 mb level to about 700 mb. The second case is also a simulation from the same model but is a patchy cumulus situation based on Atlantic Trade wind Experiment (ATEX) data. The domain where the simulated clouds reside is 5 km wide and 2.5 km high.

The key ingredients of the cloud tomography technique are to probe a cloud's microwave emission from multiple directions at distinct locations and to reconstruct the internal distribution of cloud water from the resulting measurements. The microwave radiation intensity measured by radiometers, usually converted to brightness temperature for convenience, is composed of the path-attenuated emission from the background and the atmospheric emission (microwave emission of clouds, water vapor and oxygen) along the measurement path. By choosing an appropriate working wavelength, such as centimeter waves, the scattering of microwave radiation by cloud droplets and gases in the atmosphere can be neglected. So the microwave radiometer measurements depend on only the spatial distribution of atmospheric absorption coefficients. They relate to the spatial distribution of cloud water content and other atmospheric variables through the following radiative transfer equation:

$$I(\Omega_i) = I_\infty \tau(\Omega_i, 0, \infty) + \int_0^\infty B(T)\alpha(s, \Omega_i)\tau(\Omega_i, 0, s)ds\,, \qquad (1)$$

where $I(\Omega_i)$ is the radiation intensity reaching the radiometer from direction Ω_i; I_∞ is the intensity of the background microwave radiation and $\tau(\Omega_i, 0, \infty)$ indicates the attenuation of the background emission along the path specified by direction Ω_i; $B(T)$ is the Planck function at temperature T; α is the absorption coefficient determined by the atmosphere state; and $\tau(\Omega_i, s_1, s_2) = \exp[-\int_{s_1}^{s_2} \alpha(s, \Omega_i)ds]$ is the transmission between two points s_1 and s_2 on the path along direction Ω_i.

A real radiometer measurement $\bar{I}$ is the convolution of I with the antenna gain pattern G, which is determined by the size and shape of the antenna and can be characterized by antenna beam with. In this study, the antenna gain pattern is assumed to be the widely used form that decreases exponentially with the square of angular departure from the center axis Ω_i (Drake and Warner, 1988),

$$\bar{I}(\Omega_i) = \int I(\Omega) G(\Omega - \Omega_i) d\Omega, \quad G(\xi) = \frac{1}{w}\left(\frac{4\ln 2}{\pi}\right)^{1/2} \exp\left[-4\ln 2\left(\frac{\xi}{w}\right)^2\right]. \tag{2}$$

Here w stands for the width of the antenna beam between rays where the gain is half its maximum value.

Substituting Eq. (1) into Eq. (2), taking into account the equality $\tau(\Omega_i, s_1, s_2) = \tau(\Omega_i, s_1, s)\tau(\Omega_i, s, s_2)$, and approximating the angular integral using the Gauss quadratures, we get:

$$\begin{aligned} &\sum_{k=1}^{N_H} w_k \tau(\Omega_{ik}, 0, s_1) \int_{s_1}^{s_2} B\alpha\tau(\Omega_{ik}, s_1, s) ds = \bar{I}(\Omega_i) - \sum_{k=1}^{N_H} w_k I_\infty \tau(\Omega_{ik}, 0, \infty) \\ &- \sum_{k=1}^{N_H} w_k \left[\int_0^{s_1} B\alpha\tau(\Omega_{ik}, 0, s) ds + \tau(\Omega_{ik}, 0, s_2) \int_{s_2}^{\infty} B\alpha\tau(\Omega_{ik}, s_2, s) ds\right] \end{aligned}. \tag{3}$$

Here N_H is the number of the Gauss quadratures; w_k is the weight of the antenna gain pattern corresponding to the Gauss quadratures; s_1 and s_2 are the path lengths from the radiometer to the locations at which the ray with direction Ω_i enters and leaves the cloud.

Given a total number of m rays, Eq. (3) can be further discretized by dividing a domain, which is large enough to contain the interested clouds, into $n=N^3$ (N^2 for a 2D slice) equal- sized pixels to yield the following matrix equation:

$$\mathbf{Ax}=\mathbf{b}, \tag{4}$$

where $\mathbf{x}^T=(\alpha_1,\alpha_2,\cdots,\alpha_n)$ is the vector of absorption coefficients; $\mathbf{b}^T=(b_1,b_2,\cdots,b_m)$, is the vector of adjusted measurements, b_i equals the right side of Eq.(3) and can be interpreted as the microwave emissions along the path from cloud liquid water and other absorptive agents plus the path-attenuated background emission; and $\mathbf{A}=(a_{ij})$ is an m×n matrix with

$$a_{ij}=\sum_{k=1}^{N_H} w_k \tau(\Omega_{ik},0,s_1)\int_{s_1}^{s_2} B\varphi_j(s,\Omega_{ik})\tau(\Omega_{ik},s_1,s)ds. \tag{5}$$

$\varphi_j(s, \Omega_{ik})$ is nonzero only if the point (s, Ω_{ik}) is in the jth cloud pixel, and there $\varphi_j=1$.

As shown in Part I, the tomographic retrieval problem is actually the inversion of the matrix equation (4) for the vector of absorption coefficients. Atmospheric absorption coefficient in turn is determined by the distribution of the absorption coefficients of the atmosphere. In clouds, the absorption coefficient consists generally of contributions from liquid water (α_l), water vapor (α_v), and molecular oxygen (α_{O2}). The formulae for calculating absorption coefficient for non-precipitating clouds, given state variables of the atmosphere, are those of Westwater (1972) and Falcone (1966); they are also

specified in the Appendix of Warner et al. (1985). The absorption coefficient is simply a linear function of LWC,

$$\alpha = \kappa_l \cdot LWC + \alpha_v + \alpha_{O2}, \tag{6}$$

where κ_l is the absorption efficiency of liquid water and depends only on temperature, and radiometer frequency. Our previous studies shows that the retrieval error associated with the uncertainties in humidity and temperature measurements is negligible with current radiosonde technique. Thus, for simplicity, we assume the distributions of water vapor and atmospheric temperature are known exactly in this study.

To summarize, the observation system simulation experiment is composed of the following steps: (1) specifying the atmospheric state, choosing appropriate radiometer specifications and data collection strategy (e.g., radiometer scanning speed, platform moving speed); (2) simulating the radiometer measurements using the radiative transfer equation (2); (3) inverting the simulated radiometric data to reconstruct the distribution of microwave absorption coefficient and then calculating the distribution of cloud liquid water content using Eq. (6).

3. Comparison of L_1 and L_2 regularizations

As shown in our previous studies, the retrieval problem of cloud tomography, i.e., the inversion of Eq. (4) for vector **x**, is highly ill-posed because of limited radiometer view of clouds (an ideal tomographic reconstruction would require a cloud to be scanned from all directions in a 4π sphere centered at the cloud). Regularization techniques that make use

of various types of *a priori* knowledge should be used to obtain more physically creditable retrievals (Twomey, 1977). As shown in Part I of this paper, the regularization of the equation (4) in the form of *Lp* norm can be written as,

$$\min_x \left\{ \|\mathbf{x}\|_p \right\}, \text{ subject to } \|\mathbf{Ax} - \mathbf{b}\|_2^2 \le \varepsilon \text{ and } o\text{ther constraints}. \quad (7)$$

The notation $\|\cdots\|_p$ stands for the *Lp* norm of a vector, and ε is an error tolerance usually determined by the measurement error and the error associated with the forward radiative transfer model. In this section we examine the skills of two different regularization techniques: the standard Tikhonov regularization that corresponds to p=2 (L_2 norm), and the total variation (TV) regularization that corresponds to p=1 (L_1 norm).

The linear L_2 norm regularization is widely used in many disciplines, and it is relatively easy for numerical implementation because of its linearity (Hansen, 1998). But the L_2 norm usually penalizes more when the gradients are large, and thus it tends to bias toward a smooth solution (Strong and Chan., 2003). One of our previous study shows that this method often fails to capture some discontinuous structures around cloud top where cloud water content decreases from its maximum value to zero in a few tens of meters, instead the retrieved cloud top boundaries are often blurred and extended to higher altitudes (Huang et al., 2008b). Another option is non-linear L_1 norm regularization such as the TV regularization. The main advantage of the TV regularization is that it doesn't penalize discontinuities in the solution, while simultaneously not penalizing smoothness in the solution; thus under certain conditions it can preserve the exact discontinuous edge in the solution (Acar and Vogel, 1994;

Chambolle and Lions, 1997). Let us use a simple example first present in Pederson (2005) to illustrate the point. Inspecting the piecewise linear function illustrated in Figure 2, we can calculate the *Lp* norm (raised to the power *p*) of the gradient of *f*(*t*) as follows:

$$\begin{aligned} \left\| f'(t) \right\|_{\mathrm{p}}^{\mathrm{p}} &= \int_{-\infty}^{+\infty} \left| f'(t) \right|^{p} dt \\ &= \int_{0}^{h} \left(\frac{d}{h} \right)^{p} dt \\ &= d^{p} h^{1-p} \end{aligned} \tag{8}$$

Hence for *p*=1 (the TV regularization), we have

$$\left\| f'(t) \right\|_{1} = d \, .$$

And for *p*=2 (the standard Tikhonov regularization),

$$\left\| f'(t) \right\|_{2}^{2} = d^{2} h^{-1} \, .$$

This means that if *p*=1, we see that the width of the interval *h* has no influence on the regularization term; thus the TV regularization should have no preference the scale of the structure. On the other hand, for *p*=2 it is easy to verify that the smaller *h* is, the larger the regularization term becomes. So the Tikhonov method tends to suppress the large discontinuities at small scales and thus is likely to pose a poor capability of capturing high-frequency structure (Strong and Chan, 2003). However, the TV regularization can be numerically difficult to implement and also computationally expensive because of its nonlinearity.

The linear Tikhonov method can be implemented in a direct manner by calculating the inverse kernel matrix, such as the singular value decomposition method (Hansen,

1998). Both the Tikhonov and the TV regularization problems can also be solved in an iterative manner, such as the widely used algebraic reconstruction technique (Gordon et al., 1970; Twomey, 1987). In part I of this paper, we present an iterative algorithm that can determine the weight of the regularization term adaptively. Here we carry out a test to verify whether the iterative retrieval algorithm present in Part I of this paper yield the same solution as the direct inversion method. The reference cloud cases are the stratocumulus and broken cumulus clouds described in Section 2 (Figure 2). A virtual airborne cloud tomography setup is used to produce the simulated tomographic data (more details on the specifications of the airborne tomography setup can be found in Section 3). The direct and iterative retrieval algorithms are then used to invert the simulated tomographic data. The difference between the retrievals from the two retrieval algorithms is negligible for both cloud cases. In the rest of our observation system simulation experiments, we use the iterative algorithm because it doesn't require multiple retrieval runs to determine the optimal weighting parameter for the regularization.

We then conduct four observation system simulation experiments using the airborne cloud tomography setup with various combinations of cloud case and regularization technique (two cloud cases and two regularization methods). Figure 4 shows the retrieved cloud images with the standard Tikhonov regularization, and TV regularization. The root mean squared difference between the retrieval of Tikhonov regularization and the reference is 0.09 gm^{-3} for the stratocumulus cloud case and 0.03 gm^{-3} for the broken cumulus case. For both cloud cases, the Tikhonov retrieval reconstruct the cloud field with reasonable fidelity; the location and shape of clouds are well reproduced. As expected, the Tikhonov method appears to smooth out the sharp cloud top boundary

where the largest discontinuity of cloud liquid water content occurs; as a result, the retrieved cloud top is extended to a much higher altitude for both cloud cases. Also some scattered clouds with very low water content appear in some regions that are clear sky at the reference images, possibly associated with the random noises imposed to the simulated radiometric data. When the TV regularization is used, the retrieval error for both cloud cases is reduced significantly; it becomes 0.065 gm^{-3} for the stratocumulus and 0.02 gm^{-3} for the broken cumulus. The dramatic reduction in retrieval error indicates the L_1 norm TV regularization is superior to the L_2 norm Tikhonov regularization in solving ill-posed cloud tomography problem. The cloud fields are reproduced with higher fidelity compared with the Tikhonov retrievals. The sharp cloud top edges now are well reproduced in the retrieval, clearly showing the superior skill of the TV regularization in preserving discontinuous structure in the original images.

4. Results of sensitivity studies

In this section, we conduct a group of sensitivity studies by means of observation system simulation experiments to investigate the effects of a variety of factors on the tomographic retrieval and thus to determine the optimal tomographic configuration and data acquisition strategies. The factors examined include radiometer characteristics, radiometer scan strategy, background microwave property, and platform speed and height.

4.1 Ground-based and airborne setups

There are several important differences between ground- and aircraft-based cloud tomography setups; among are platform moving speed and background microwave

brightness temperature. For a ground-based cloud tomography setup the speed of a truck trailer is typically on the order of a few tens of miles per hour (mph), while the speed of an aircraft is usually a few hundreds of mph. The difference in platform moving speed can result in very different data geometries and thus can impact the retrieval accuracy in a significant way. Another major difference between the two setups is that the ground radiometer views the upper hemisphere to measure clouds while the airborne radiometer usually scans clouds in the lower hemisphere due to the limitation of aircraft design. A direct consequence of this is that the microwave contrast between clouds and the background will be very different for these two setups. For the ground-based setup, the cosmic background is well known to be around 3.0 K and in a strong contrast with clouds. For the aircraft-based setup, the background is either land surface or sea surface and the brightness temperature ranges from 150 K to 250 K in the microwave Ka band, which is less distinctive with clouds. In this research we consider only sea surface background in the airborne tomography simulations because the high emissivity of land surface makes them almost undistinguishable from warm clouds. The directional distribution of sea surface microwave emission is simulated by a two-scale thermal emission model (Johnson, 2006).

Table 1 shows the typical values of radiometer and platform specifications of the two tomographic setups; these values are used throughout the sensitivity studies if not specified explicitly. The radiometer is assumed to have a 0.5 K random noise with 2.3 degrees beam width. Each radiometer scan cycle takes 43 seconds and only the rays within 80 degrees off the nadir or zenith are considered as a valid measurement (ground clutters and water vapor could cause problems if the beam were too close to horizon).

The background brightness temperature is 3 K for the ground-based configuration, and a 0.5 K random noise is also imposed to the background in all simulation experiments. For the airborne configuration, the background brightness is strongly depended on the incident angle and is simulated by a two-scale sea surface thermal emission model by assuming a 283 K surface temperature. A 0.5 K random noise is also imposed to the sea surface brightness temperature. The moving speed of the ground-based platform is assumed to be 24 m/s (53.7 mph), while the aircraft is assumed to fly at a speed of 96 m/s (172.3 mph) at an altitude of 3500 meters.

We perform four system simulation experiments using the two cloud cases described in Section 2 for each of the two mobile tomography setups. All the parameters of the ground-based and airborne setups are identical except for the background brightness temperature, platform altitude, and the platform moving speed. Figures 5 and 6 show the cloud fields retrieved using the two tomography setups along with their corresponding retrieval error images. For the stratocumulus cloud case, the retrieval error of the airborne setup (0.061 gm^{-3}) is 50% higher than the error of the ground-based setup (0.041 gm^{-3}). The ground-based retrieval accurately reproduces the base and top of the stratocumulus clouds, while the retrieval from the airborne setup shows more spurious scattered clouds at clear sky regions (Figure 5). And for the patchy cumulus case, the result is very similar: the retrieval error of the ground-based setup is 0.006 gm^{-3}, substantially lower than the retrieval error of the airborne setup (0.02 gm^{-3}). The airborne retrieval shows some puffy clouds with low water content at several clear sky regions, while the ground-based retrieval reproduces the original image with such a high fidelity that one can hardly tell

their difference (Figure 6). The reason why the ground-based setup is superior to the aircraft-based setup will be discussed in Sections 4.3 and 4.4.

4.2 Radiometer noise

The second factor examined is the radiometer noise level. The experiment is based on the stratocumulus cloud case. Figure 7 shows that the retrieval error for both the ground-based and airborne configurations increases monotonically with the radiometer noise level, as one would expect. The rate of increase of the retrieval error diminishes with the noise level. The retrieval error of ground-based setup increases by a factor of 3 from 0.036 gm^{-3} to 0.12 gm^{-3} when the radiometer noise level increases from 0.1 K to 6.0 K. And for the airborne setup, the retrieval error increases from 0.06 gm^{-3} to 0.15 gm^{-3}. The noise level of modern microwave radiometers is typically in the range of 0.1 K to 0.5 K; according to Figure 7, they can provide retrievals accurate to within 5% of the maximum cloud water content. Even when the noise is extremely high (>4 K), the simulations show that the tomographic retrievals can still roughly reproduce some of the cloud features but the resolving of high-frequency structure is difficult because the retrievals rely more on the arbitrary mathematical constraints.

4.3 Uncertainty in the brightness temperature of background

The third factor considered in this research is the uncertainty in the estimate of background radiometric characteristics, i.e., the cosmic brightness temperature for the ground-based setup and the sea surface brightness temperature for the airborne setup. For the ground setup, the cosmic background is well-known to be around 3 K, but the water

vapor emission between cloud top and the top of atmosphere also contribute to the path-integrated radiometer measurements and thus should be considered as a part of background emission. Accounting for this, we set the background brightness temperature of the ground-based setup to be 20 K and impose varying levels of uncertainty (from 0.1 K to 6 K) to the background. The sea surface microwave emission is a function of incident angle and the angular distribution is determined by surface roughness and the orientation of sea waves (Johnson, 2006). For example, wind-caused wave and foam can lead to an uncertainty up to 3 K in the simulation of directional brightness temperatures. Figures 8 shows that the uncertainty in the background brightness temperature has similar effects on the retrieval as the noise in the radiometric measurements. The retrieval error increases with background uncertainty, while the rate of this increase diminishes with the background uncertainty.

The microwave contrast between the cosmic background and clouds is much greater than the contrast between sea surface and clouds. So the signal-to-noise ratio of the ground-based setup will be higher than that of the airborne setup if the radiometer noise is the same. Furthermore, the background uncertainty of the airborne setup is usually much higher than that of the ground-based setup because of the large uncertainty associated with the measurements of sea surface emission or the simulation of wind-driven sea surface waves. Therefore, the result of Section 4.1 that the ground-based retrieval is much more accurate than the airborne retrieval can be partly attributed to their differences in the characteristics of background emission.

4.4 Scan strategy

It is shown in our previous studies that beam intersection is crucial to the success of a tomographic reconstruction. If successive scans don't overlap with each other, one will be able to retrieve only the path-integrated cloud water content for each beam. The radiometer scanning speed or the duration of a scan cycle is important to the geometry of the tomographic data; it is a key factor that determines to what extent the microwave beams from successive scan cycles intersect with each other.

Figure 9 illustrates that the retrieval error increases monotonically with radiometer scanning speed. For the ground-based configuration, the retrieval error varies by a factor of 4 from 0.032 gm^{-3} to 0.13 gm^{-3} when the duration of radiometer scan cycle changes from 10 seconds to 160 seconds. For the airborne configuration, the retrieval increases by a factor of 3 from 0.045 gm^{-3} to 0.14 gm^{-3} with the same change of radiometer scanning speed. This result can be explained by two facts. First, there will be more scan cycles if the radiometer scan faster since the total time needed to pass the interested clouds depends only on the platform speed. Second, with a faster radiometer, two successive cycles will be closer to each other in distance and thus the swath of each scan cycle will overlap more with its previous and succeeding scan cycles. Therefore, from the perspective of data geometry, fast scanning radiometers are preferred in tomographic applications. On the other hand, a faster scan means shorter integration time for each beam and thus greater random noise in data, which will adversely affect the retrieval accuracy. The optimal choice of radiometer scanning speed can be found by taking both factors into account.

4.5 Platform moving speed

Platform moving speed, similar to radiometer scanning speed, is a key factor that determines how many scan cycles the radiometers have while passing the interested clouds and determines the distance between successive scans. If the platform moves so fast that successive scans are well separated with each other and don't overlap, it will be almost impossible to reconstruct the cloud structure from the radiometric measurements. As illustrated in Figure 10, a reduced platform speed substantially improves the retrieval accuracy for both the ground-based and airborne configurations. For the ground-based setup, the retrieval error increases from 0.036 gm^{-3} to 0.073 gm^{-3} when the platform speed varies from 24 m/s to 96 m/s. Similarly, for the airborne configuration, the realistic range of platform speed is from 64 m/s to 240 m/s and correspondently the retrieval error change from 0.049 gm^{-3} to 0.12 gm^{-3}. When the platform moves slowly, the swath of each scan cycle will overlap significantly with its successive scans (and also the previous scans) and thus there will be sufficient intersected beams for retrieving cloud structure. When the platform speed exceed 200 m/s (each scan cycle at best overlaps with its previous and succeeding scan cycles), the tomographic retrieval will become very difficult because of the very limited beam intersection.

The typical speed of a research aircraft is 200-300 mph, almost one order faster than that of a ground-based platform. This provides another explanation for the result in Section 4.1 that the ground-based setup substantially outperforms the airborne setup.

However, a slower moving platform means that it will take a longer time to acquire the necessary data. The life time of clouds is on the order of tens of minutes and a cloud can evolve significantly in a few minutes. So, practically, there is always a trade-off

between choosing a slower platform (thus it takes longer to finish the measurements) and minimizing the cloud evolution during the measurement.

4.6 Platform altitude

The geometry of tomographic measurements, specifically the range of radiometer view angle (indicated by Ω in Figure 11), often plays an important role in determining the total amount of useful information in the tomographic measurements. In general, the larger the angle Ω spanned by the radiometer rays (those hitting the interested cloud), the more useful information in the resultant measurements. An ideal tomographic reconstruction would require the target to be viewed from all directions, i.e., the range of view angle should be 360 degrees. In cloud tomography applications, the range of view angle Ω is usually less than 140 degrees and as a consequence the retrieval problem becomes highly ill-posed. The range of view angle is often limited by the platform altitude as shown in Figure 11. When the platform altitude is much higher than that of the cloud to be measured, the platform needs to move a large distance in order to cover a useful range of view angle (thus it will increase the measurement time).

Figure 12 shows that the retrieval error increases when the aircraft altitude increases from 2.5 to 8 km (cloud top is about 2.2 km). This result is consistent with the fact that the range of view angle decreases with platform height if the total measurement time (thus the distance the aircraft travels) is fixed. The retrieval error increases by a factor of two from 0.07 gm^{-3} to 0.13 gm^{-3} while the aircraft altitude changes from 2.5 km to 7 km. The optimal aircraft altitude seems to be between 2.8 to 3.5 km. If the aircraft is beyond the 5.5 km altitude, the retrieval of the airborne setup can hardly reproduce the cloud top

boundary, indicating the lack of information in the tomographic measurements to resolve the cloud structure. When the aircraft is close to cloud top (within 2.8 to 4.5 km), both the cloud base and top boundaries are reproduced accurately. But if the aircraft is too close to cloud top (<2.5 km), the scan cycles will have no or little overlapping at the regions around cloud top; so the tomographic data again will not hold enough information content to retrieve cloud structure around cloud top.

5. Conclusions

Part I of this research examines the results of a very limited cloud tomography experiment during the 2003 AMSR-E validation campaign at Wakasa Bay and demonstrates that the tomographic method is capable of retrieving cloud water distribution using only a single scanning microwave radiometer aboard a research aircraft. It is found that during the Wakasa Bay experiment many conditions were not optimal for cloud tomography retrieval, such as high aircraft altitude and speed, strong surface wind (thus large uncertainty in the estimate of sea surface thermal emission). Part II (this paper) then focuses on a group of sensitivity studies to investigate the factors that are responsible for the retrieval quality of cloud tomography.

We conduct a series of observation system simulation experiments either by varying the specifications of the cloud tomography configuration or by choosing different inversion techniques. Two inversion techniques are examined: the first one is based on the Tikhonov regularization (L_2 norm) and the other is based on the total variation regularization (L_1 norm). The retrieved cloud water content from the Tikhonov regularization method is accurate to within 10% of the maximum value in the cloud and captures most of the features of cloud field in the original image. Nevertheless, the

retrieval cloud top boundary appears to be much smoother than that in the original image; this concurs with the results from our previous studies that the L_2 norm regularization can hardly preserve structure where large discontinuity occurs. The retrieval from the L_1 norm total variation regularization shows some noticeable improvements over its L_2 norm counterpart. The retrieval error is significantly reduced. The sharp cloud edges are well captured and some other cloud features are also reproduced with high fidelity.

The observation system simulation experiments show that, besides the choice of inversion technique, the retrieval accuracy also depends on many other factors like radiometer characteristics, scanning strategy, platform moving speed, and platform altitude. A typical ground-based cloud tomography setup substantially outperforms an airborne setup with the same radiometer specification. The reason relies on two facts: (1) the ground-based setup is slower and thus allows for more scan cycles and better beam intersection than the airborne one; (2) the microwave contrast between clouds and the cosmic background is much greater than that between clouds and the sea surface, so the ground-based setup usually has higher signal-to-noise ratio. The retrieval error increases with the radiometer noise level and the uncertainty in the knowledge of background brightness temperature, as one would expect. The radiometer scan strategy, i.e., fast versus slow scanning, is another factor playing an important role in determining the tomographic retrieval quality. Fast scanning means more scan cycles and better overlapping between the swaths of successive scan cycles if other conditions are the same, and thus it will lead to improved retrievals. The moving speed of the platform is also a critical parameter to tomographic measurements. A slow platform allows for more scanning data and better overlapping between the swaths of the radiometer scan cycles.

Thus, in this respect, a slow platform is favorable to cloud tomography. On the other hand, clouds evolves at the same time the radiometric measurements are taken and thus a fast platform has the advantage in minimizing the adverse influence of cloud evolution on cloud tomography retrieval. The altitude of the aircraft is another important parameter to the geometry of the tomographic measurements. The simulation experiments show that the optimal aircraft height is about 0.5 to 1 km over cloud top. When the aircraft altitude relative to the cloud top becomes comparable with the cloud size, the range of radiometer view angles will be limited and thus the accurate retrieval of cloud structure will be difficult.

Acknowledgements

This work has been supported by the DOE Atmosphere Radiation Measurement program under Contract DE-AC02-98CH10886. We thank Drs. Emil Sidky, Yangang Liu, and Michael Jensen for many insightful discussions that help to improve this study.

References

Acar, R., and C. R. Vogel (1994): Analysis of total variation penalty methods. *Inv. Prob.*, vol. 10, pp. 1217–1229.

Ackerman, S.A., O.B. Toon, and P.V. Hobbs (1995): A model for particle microphysics, turbulent mixing, and radiative transfer in the stratocumulus topped marine boundary layer and comparisons with measurements. *J. Atmos. Sci.*, 52, 1204-1236.

Chambolle, A., and P. L. Lions (1997): Image recovery via total variation minimization and related problems. *Numer. Math*., vol. 72, pp. 167–188.

Drake, J.F., and J. Warner (1988): A theoretical study of the accuracy of tomographic retrieval of cloud liquid with an airborne radiometer. *J. Atmos. Sci. Ocean. Tech*., 5, 844-857.

Falcone, V. (1966): Calculation of apparent sky temperature at millimeter wavelengths. *Radio Sci*., 1 (new series), 1205-1209.

Frisch, A.S., C.W. Fairall, and J.B. Snyder (1995): Measurement of stratus cloud and drizzle parameters in ASTEX with a Ka-band Doppler radar and a microwave radiometer. *J. Atmos. Sci.*, 52, 2788–2799.

Gordon, R., R. Bender and G. T. Herman (1970): Algebraic Reconstruction Techniques (ART) for Three-dimensional Electron Microscopy and X-ray Photography. *J. Theor. Biol*., 29, 471-481

Hansen, P.C. (1998): *Rank deficient and ill-posed problems: Numerical aspects of linear inversion*. SIAM, Philadelphia, pp. 247.

Hogan, R. J., N. Gaussiat and A. J. Illingworth (2005): Stratocumulus liquid water content from dual-wavelength radar. *J. Atmos. Oceanic Technol.,* 22, 1207-1218.

Huang, D., Y. Liu, and W. Wiscombe (2008a): Determination of cloud liquid water distribution using 3D cloud tomography. *J. Geophys. Res.*, 113, D13201, doi:10.1029/2007JD009133.

Huang, D., Liu, Y., and Wiscombe, W. (2008b): Improving the tomographic retrieval of cloud water distribution using constrained algorithms. *J. Geophys. Res*., accepted.

Johnson, J.T. (2006): An efficient two-scale model for the computation of thermal emission and atmospheric reflection from the sea surface. *IEEE Trans. Geosci. Remote Sens*., 44, 560–568.

Liljegren, J., E. Clothiaux, G. Mace, S. Kato, and X. Dong (2001): A new retrieval for cloud liquid water path using a ground-based microwave radiometer and measurements of cloud temperature, *J. Geophys. Res*., 106, 14,485-500.

Lobl, S. E., K. Aonashi, B. Griffith, C. Kummerow, G. Liu, M. Murakami, and T. Wilheit (2007): Wakasa Bay --- An AMSR Precipitation Validation Campaign. *Bull. Amer. Met. Soc*., 88, 551-558

Pederson, J. (2005): Modular Algorithms for Large–Scale Total Variation Image Deblurring. Technical University of Denmark, master thesis, pp. 122.

Strong, D., and T. F. Chan (2003): Edge-preserving and scale-dependent properties of the total variation regularization. *Inverse Problems*, 19, 165-187.

Stephens, G.L. (2005): Cloud feedbacks in the climate system: a critical review. *J. Climate*, 18, 237-273.

Twomey, S. (1977): *Introduction to the mathematics of inversion in remote sensing inversion and indirect measurements*. Elsevier, Amsterdam, pp. 243.

Twomey, S. (1987): Iterative nonlinear inversion methods for tomographic problems. *J. Atoms. Sci*., 44, 3544-3551.

Warner, J., J.F. Drake, and P.R. Krehbiel (1985): Determination of cloud liquid water distribution by inversion of radiometric data. *J. Atmos. Ocean. Tech*., 2, 293-303.

Warner, J., J.F. Drake, and J.B. Snider (1986): Liquid water distribution obtained from coplanar scanning radiometers. *J. Atmos. Ocean. Tech*., 3, 542-546.

Warner, J., and J. F. Drake (1988): Field tests of an airborne remote sensing technique for measuring the distribution of liquid water in convective cloud. *J. Atmos. Oceanic Technol*., 5, 833–843.

Weare, B. C. (1996): Evaluation of the vertical structure of zonally-averaged cloudiness and its variability in the Atmospheric Model Intercomparison Project. *Journal of Climate*, 9, 3419-3431.

Westwater, E.R. (1972): Microwave emission from clouds. *NOAA Tech. Rep*. ERL 219-WPL, 18, pp. 43.

Westwater, E.R., S. Crewell, and C. Matzler (2004): A review of surface based microwave and millimeter wave radiometric remote sensing of the troposphere. *Radio Sci. Bull*., 3010, 59-80.

Table 1. The typical radiometer specifications, background characteristics, and platform parameters of the ground-based and airborne cloud tomography configurations.

	radiometer				background		platform	
	noise, K	wavelength, cm	beam width, degree	scan period, s	brightness temperature, K	uncertainty, K	speed, m/s	altitude, m
Ground-based	0.5	0.947	2.3	43	20	0.5	24	0
Airborne	0.5	0.947	2.3	43	165-180	0.5	96	3500

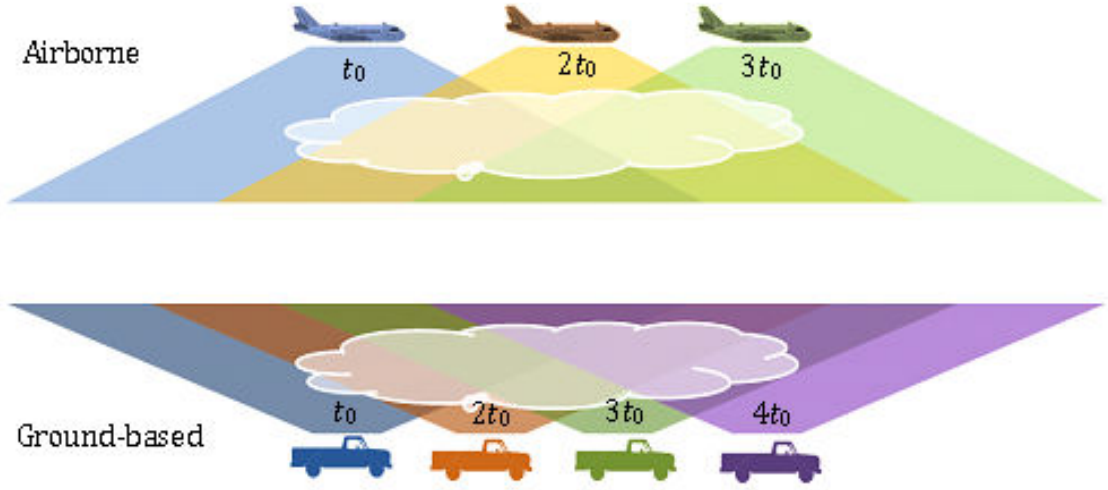

Figure 1. Illustration of the data geometry of the ground-based and airborne tomography configurations. The cartoon shows the radiometer scan swaths at time $t=t_0, 2t_0, 3t_0, \cdots$. The swath of each scan cycle is indicated by different color. The positions of the platform at time $t=t_0, 2t_0, 3t_0, \cdots$ are also shown in matching color.

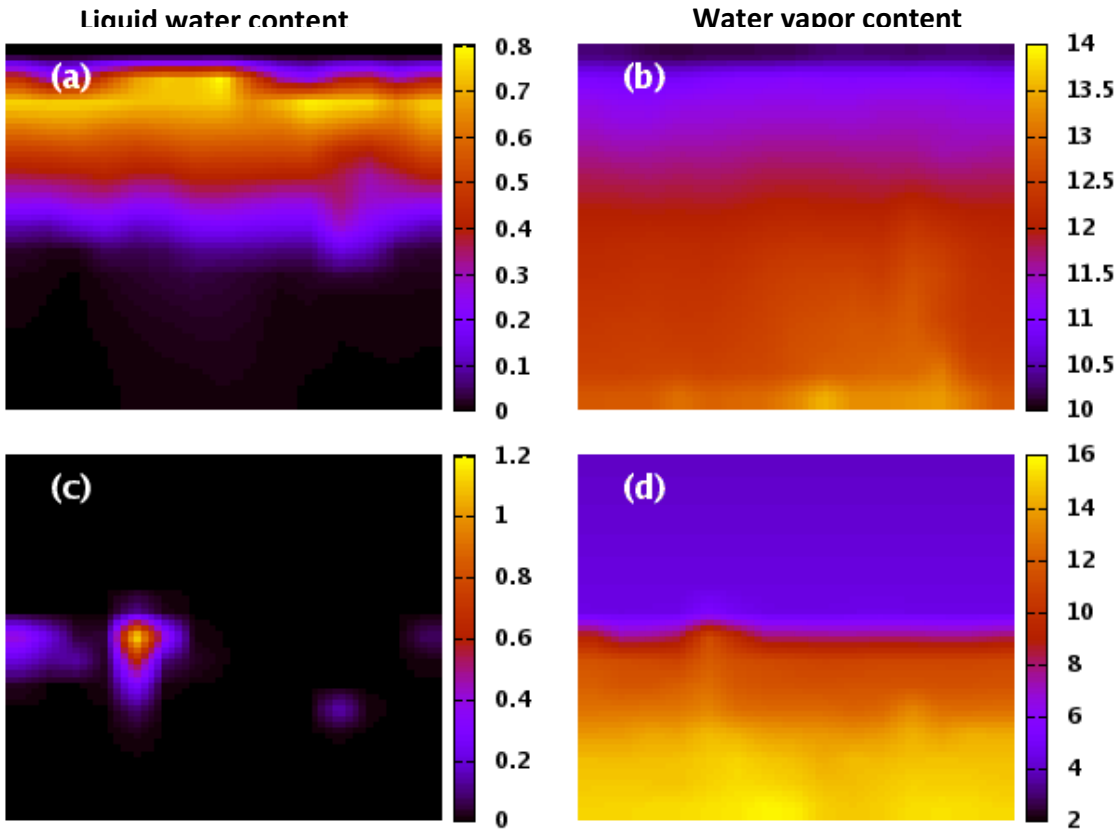

Figure 2. The cloud liquid water and water vapor fields of a stratocumulus case (ASTEX) and a puffy cumulus case (ATEX) simulated by a large eddy simulation model (Ackerman et al., 1995). (a) Stratocumulus case, liquid water; (b) Stratocumulus case, water vapor; (c) Puffy cumulus case, liquid water; and (d) Puffy cumulus case, water vapor. The domain is 5 km wide and 2.5 km high.

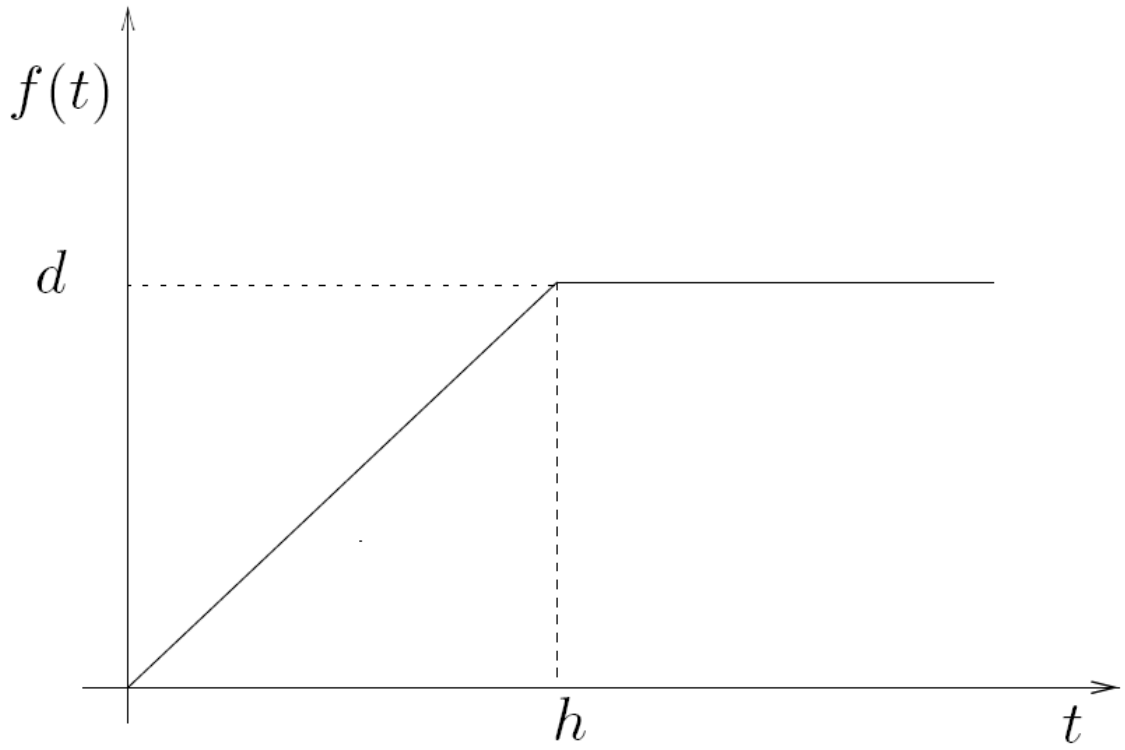

Figure 3. A piecewise linear function used to illustrate the difference between the L_1 norm total variation regularization and the L_2 norm Tikhonov regularization.

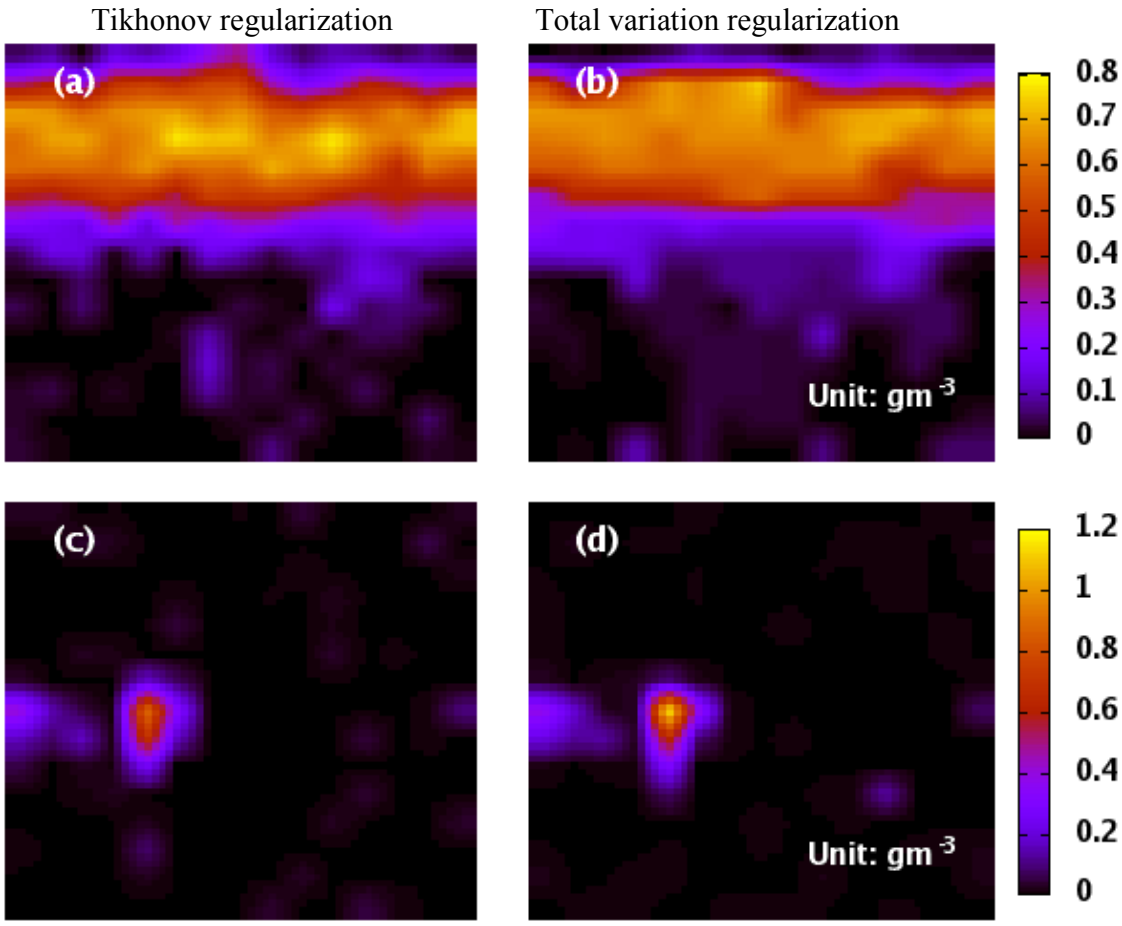

Figure 4. The cloud liquid water fields retrieved the airborne cloud tomography setup with the total variation regularization and the standard Tikhonov regularization. (a) Stratocumulus case, Tikhonov regularization; (b) Stratocumulus case, total variation regularization; (c) Puffy cumulus case, Tikhonov regularization; and (d) Puffy cumulus case, total variation regularization.

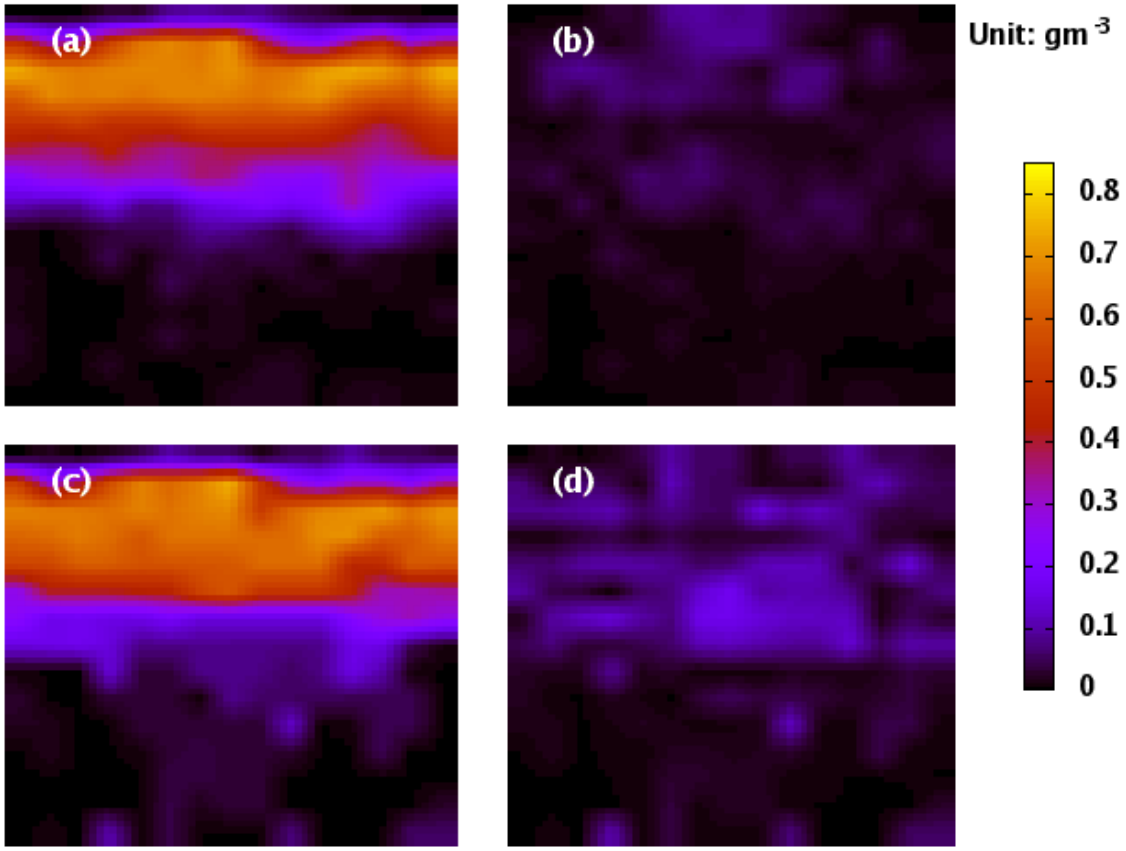

Figure 5. The retrieved stratocumulus clouds by the ground-based and airborne setups, as well as the corresponding images of error. (a) Retrieved liquid water field by the ground-based setup; (b) The error of the ground-based retrieval; (c) Retrieved liquid water field by the airborne setup; (d) The error of the airborne retrieval.

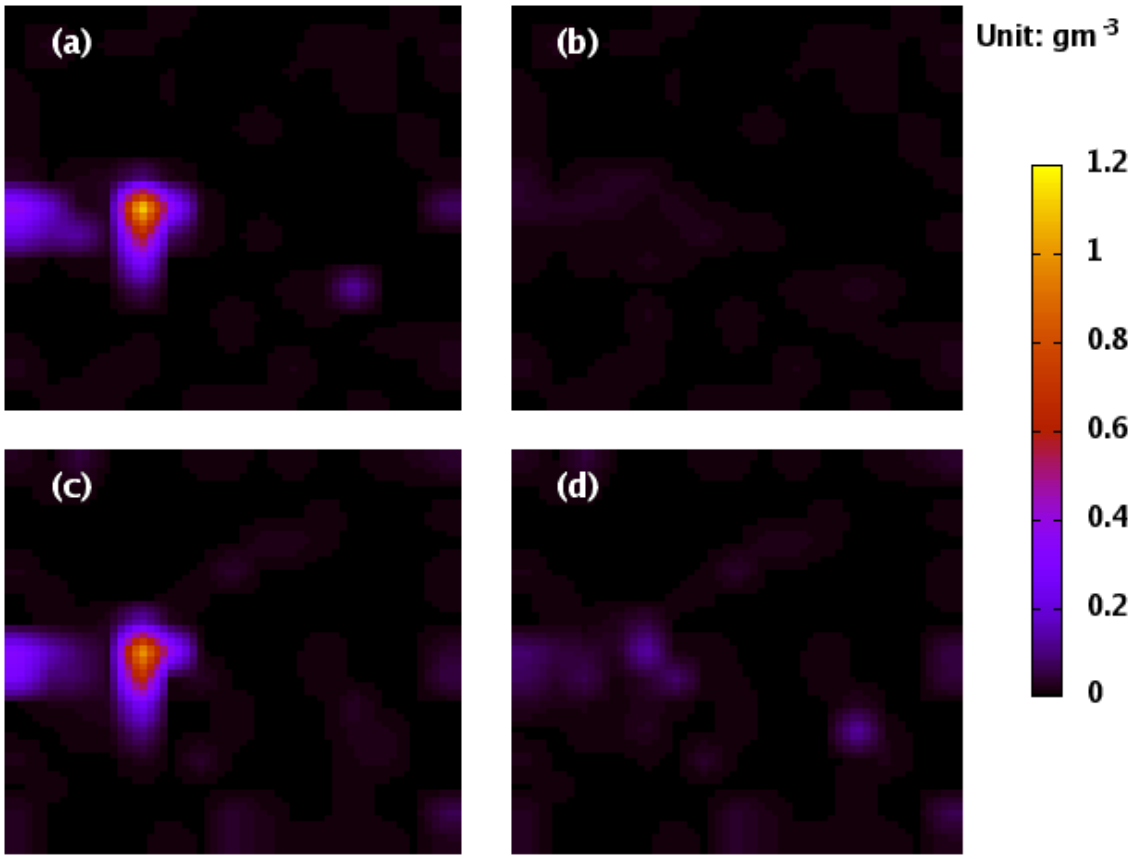

Figure 6. The retrieved puffy cumulus clouds by the ground-based and airborne setups, as well as the corresponding images of error. (a) Retrieved liquid water field by the ground-based setup; (b) The error of the ground-based retrieval; (c) Retrieved liquid water field by the airborne setup; (d) The error of the airborne retrieval.

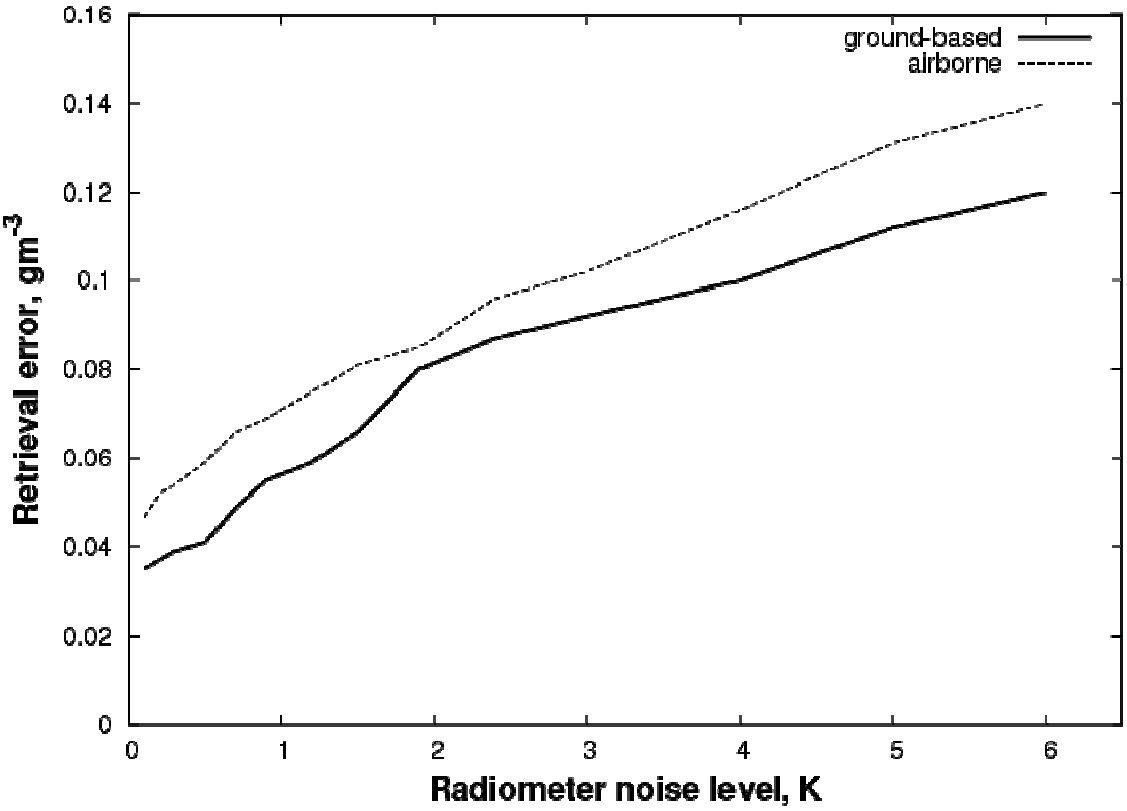

Figure 7. The retrieval error as a function of radiometer noise level. As expected, the retrieval error increases with radiometer noise for both the ground-based and airborne setups. The stratocumulus cloud case is used for this sensitivity test.

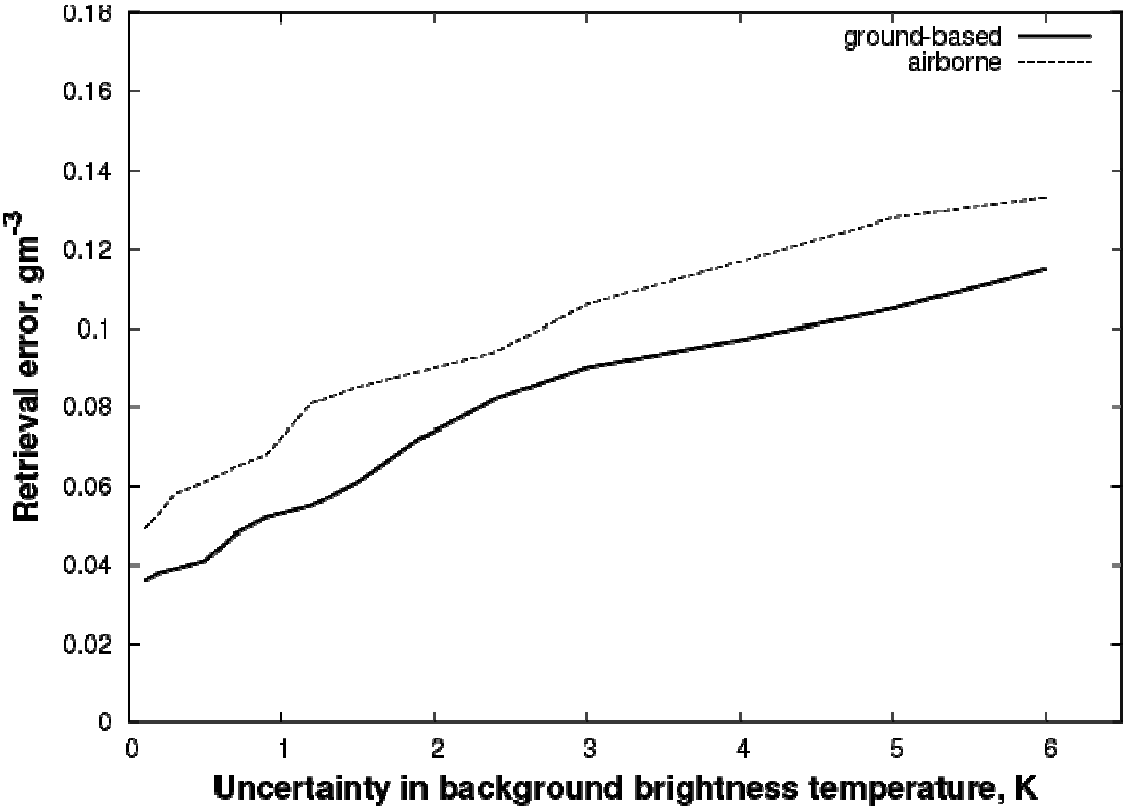

Figure 8. The retrieval error increases with the uncertainty in background brightness temperature for both the ground-based and airborne setups. The stratocumulus cloud case is used for this sensitivity test.

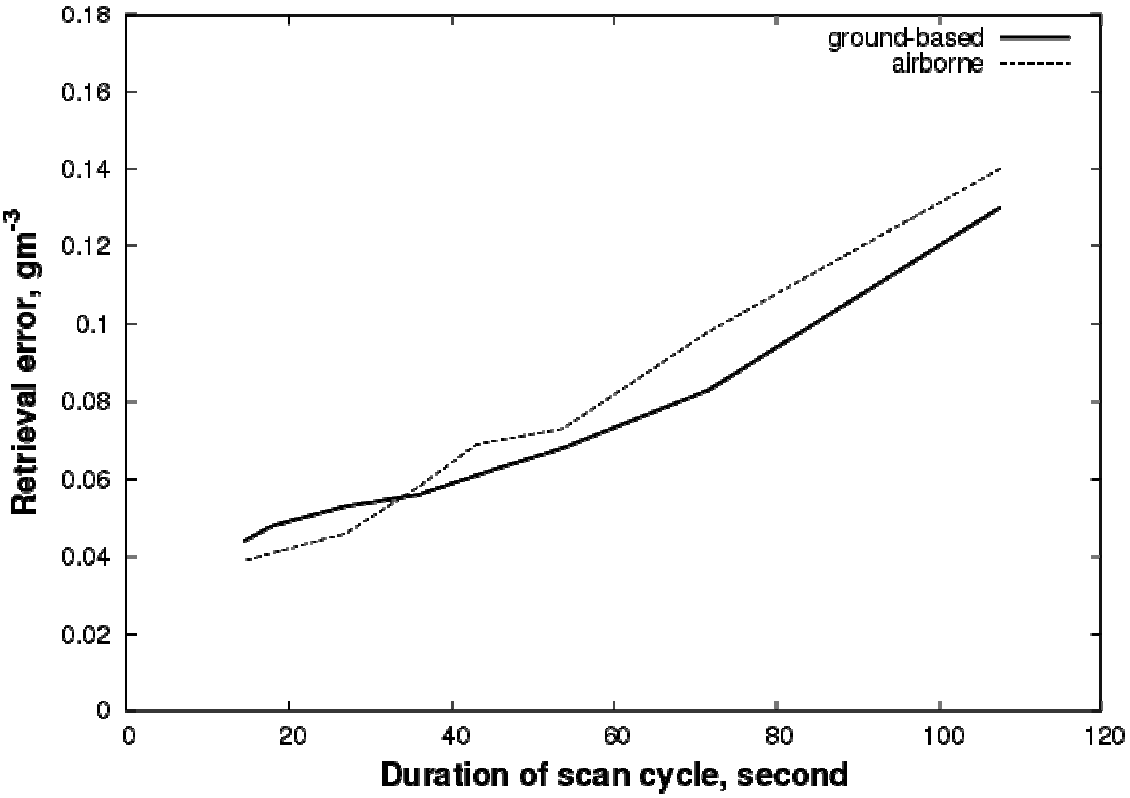

Figure 9. The retrieval error as a function of the duration of radiometer scan cycle (i.e., radiometer scanning speed). For both the ground-based and airborne setups, a faster radiometer results in better tomographic retrieval. The stratocumulus cloud case is used for this sensitivity test.

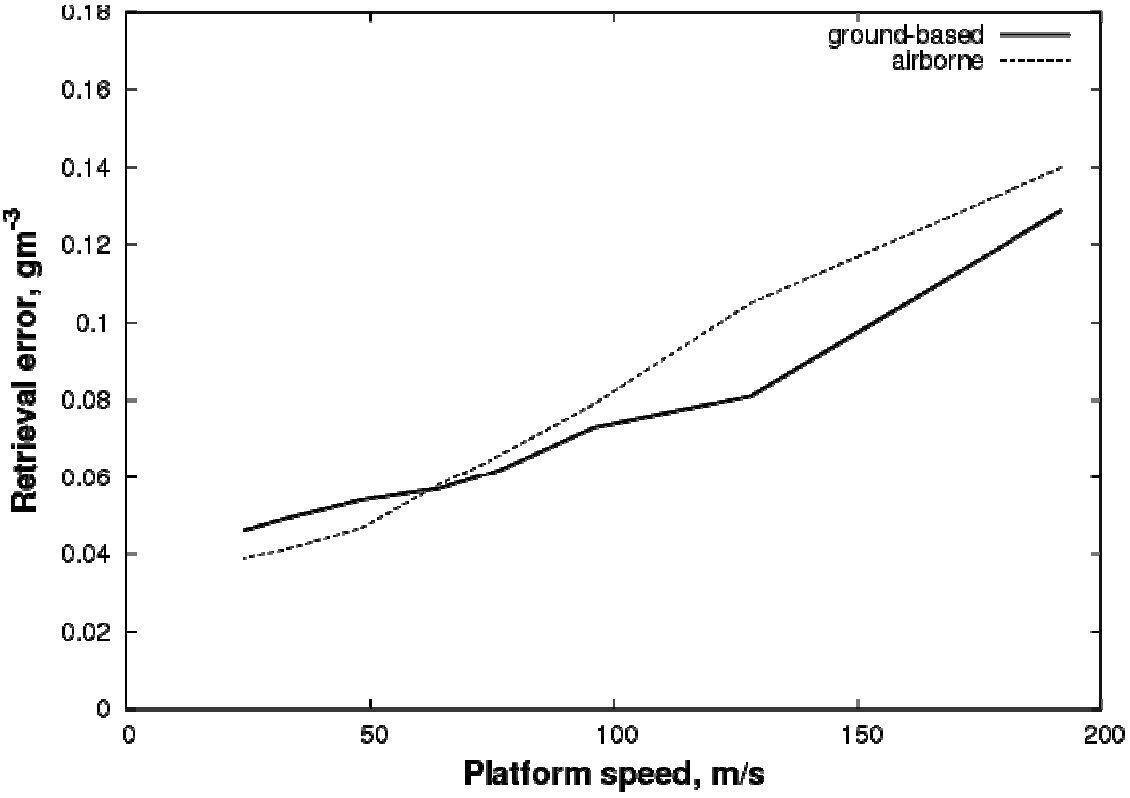

Figure 10. The retrieval error as a function of platform moving speed. A slower platform provides more accurate retrieval at the expense of longer measurement time. The stratocumulus cloud case is used for this sensitivity test.

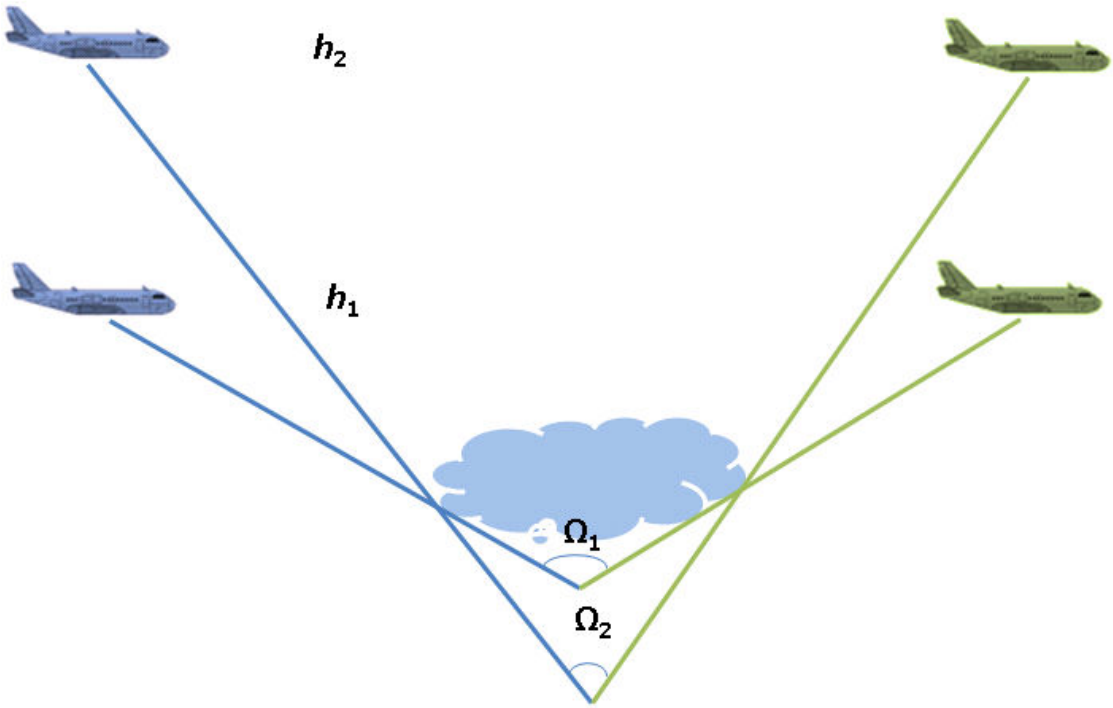

Figure 11. Illustration of the dependence of radiometer view angle on the aircraft altitude. The range of radiometer view angle (indicated as Ω_1, Ω_2) decreases with height given that the aircraft moves the same distance.

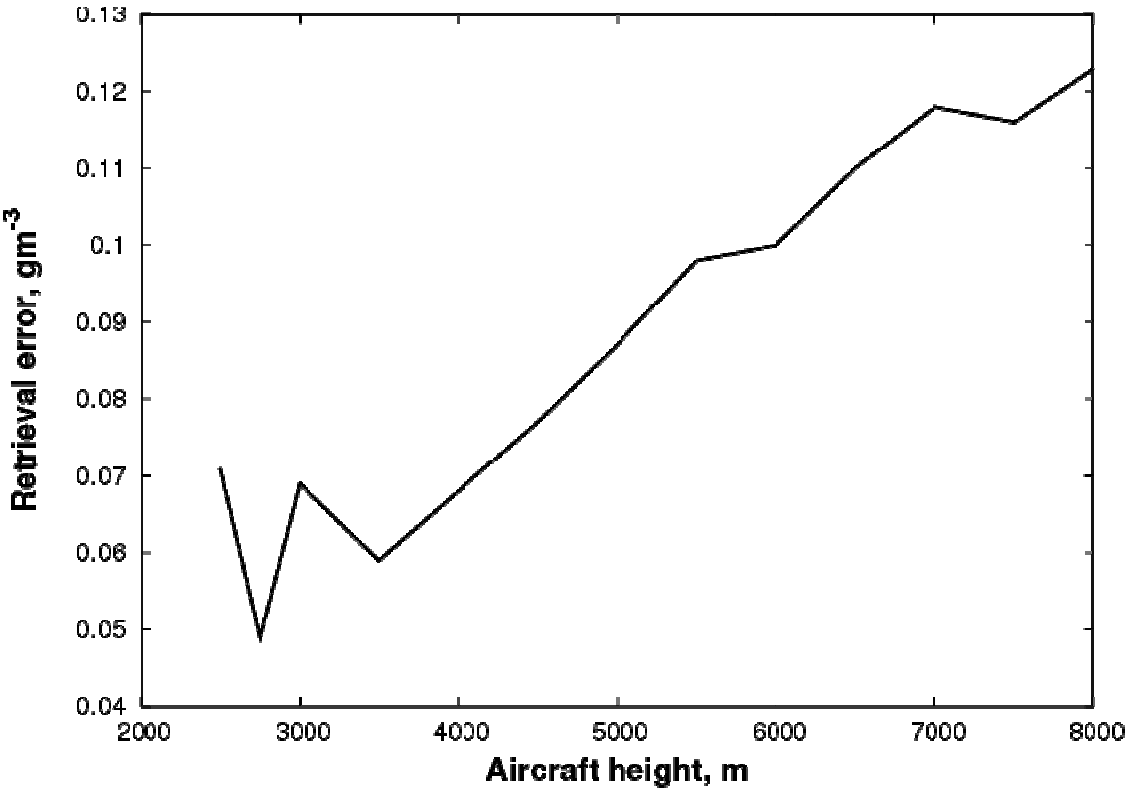

Figure 12. The retrieval error of the airborne setup as a function of aircraft altitude. The altitude of cloud top is about 2200 meters. The retrieval error first decreases with aircraft altitude, reaches it minimum when the aircraft is 500-1500 meter higher than the cloud top, and then increases with further increase of aircraft altitude. The stratocumulus cloud case is used for this sensitivity test.